Prostate Specific Membrane Antigen (PSMA)-Targeting Iron Oxide Magnetic Nanoparticles (MNPs) Enhance MRI of Preclinical Prostate Cancer

Brian Wan-Chi Tse[1], Gary J Cowin[2], Carolina Soekmadji[1], Lidija Jovanovic[1], Raja S Vasireddy[1], Ming-Tat Ling[1], Aparajita Khatri[3], Tianqing Liu[4], Benjamin Thierry[4], Pamela Joan Russell[1]

[1]*Australian Prostate Cancer Research Centre-Queensland, Institute of Health and Biomedical Innovation, Queensland University of Technology, Translational Research Institute, Brisbane, Queensland, Australia*

[2]*National Imaging Facility, Centre for Advanced Imaging, University of Queensland, Brisbane, Queensland, Australia*

[3] *Ceramisphere Pty Ltd (Health Care Division), Sydney, NSW, Australia*

[4]*Ian Wark Institute, University of South Australia, Adelaide, Australia*

Correspondence:

Pamela J Russell

pamela.russell@qut.edu.au

Telephone: +61 7 3443 7240

Fax: +61 7 3176 7440

Address: Australian Prostate Cancer Research Centre – Queensland, Institute of Health and Biomedical Innovation, Faculty of Health, Queensland University of Technology, Translational Research Institute, Level 3 West, Translational Research Institute, 37 Kent St,

Brisbane QLD 4102 Australia

ABSTRACT

Aim:

Evaluate potential of newly-developed, biocompatible iron oxide magnetic nanoparticles (MNPs) conjugated with J591, an antibody to an extracellular epitope of prostate specific membrane antigen (PSMA), to enhance MRI of prostate cancer (PCa).

Materials & Methods:

Specific binding to PSMA by J591-MNP was investigated *in vitro*. MRI studies were performed on orthotopic tumor-bearing NOD.SCID mice 2h and 24hr after intravenous injection of J591-MNPs, or non-targeting MNPs.

Results and Conclusions:

In vitro, MNPs did not affect PCa cell viability, and conjugation to J591 did not compromise antibody specificity and enhanced cellular iron uptake. *In vivo*, PSMA-targeting MNPs increased MR contrast of tumors, but not by non-targeting MNPs. This provides proof-of-concept that PSMA-targeting MNPs have potential to enhance MR detection/localization of PCa.,

KEYWORDS: Iron oxide magnetic nanoparticles (MNPs), magnetic resonance imaging (MRI), targeted nanoparticles; prostate cancer; prostate cancer specific membrane antigen (PSMA); cancer imaging; targeted imaging

INTRODUCTION

Magnetic resonance imaging (MRI) is a useful imaging tool in prostate cancer (PCa) management. It provides excellent soft tissue contrast, multi-dimensional information, does not involve exposure to ionising radiation, and is non-invasive [1]. However, like other imaging modalities such as computed tomography (CT), transurethral ultrasound (TRUS) and nuclear imaging, MRI cannot adequately detect small tumors [2]. Improvements in tumor imaging technologies are urgently required for early detection of disease, staging, and/or real-time assessment of response to therapy in PCa patients. Iron oxide magnetic nanoparticles (MNPs) have emerged as powerful contrast agents for MRI [3]. Their superparamagnetic properties make them effective at reducing transverse (spin-spin) T2-relaxation time, causing negative contrast in MR images [4, 5]. MNP-assisted MRI has the potential to improve the assessment of cell receptor expression on tumors, liver function (macrophage content and activity), inflammation, degenerative diseases, angiogenesis, perfusion and apoptosis [6]. Currently, certain iron oxide-based MNPs have been approved for use in clinical MRI, for instance ferumoxil (GastroMARK) enhance imaging of the bowel. In this study, we evaluate the potential ability of MNPs to enhance MRI of PCa. We conjugated MNPs to the prostate specific membrane antigen (PSMA)-targeting antibody, J591, via a 1,2-distearoyl-*sn*-glycero-3-phosphoethanolamine-N-[amino(polyethylene glycol) (PEG-DSPE) linkage, for delivery of the nanoparticle cargo to PCa cells. PSMA, a 750-amino acid, type 2 transmembrane glycoprotein with folate hydrolase or carboxy peptidase II activity [7], is an ideal molecular target for imaging for a number of reasons. While PSMA is expressed in normal prostate epithelial and benign hyperplastic cells, it exists as a truncated form (PSM') through alternative splicing and is found in the cytosol, whereas a transmembane form is expressed at high levels in PCa [8]. The PSMA/PSM' mRNA ratio is lowest in normal tissue and increases with increasing Gleason score [9]. PSMA expression is up-regulated in PCa, including lymph node and bone metastases, up-regulated in androgen deprivation conditions, and elevated in late stage

castrate-resistant prostate cancer (CRPC) [10-12]. In addition, PSMA has a cytoplasmic domain that contains a novel and unique amino acid sequence of MXXXL that mediates its internalisation and endosomal recycling [13, 14], which can lead to high intracellular retention of PSMA-targeting biomaterials such as MNPs. J591 was selected as the PSMA-targeting agent due to its well-established specificity. ^{177}Lu-J591 was been previously shown to target all known sites of disease in all treated PCa subjects [15], and in another study, treatment with ^{111}In-J591 and then ^{90}Y-J591 revealed 89% of known bony metastases and 69% of soft tissue lesions [16]. We provide proof-of-concept that J591-labeled MNPs can enhance MRI of orthotopic xenograft PCa in mice.

MATERIALS & METHODS

Preparation and characterisation of magnetic nanoparticles

Monocrystalline iron oxide nanoparticles were synthesized using a small modification of the solvent free one-pot procedure initially reported by Niederberger et al [17, 18]. Briefly, Fe(acac)3 powder (500 mg) was mixed with benzyl alcohol (10 mL) and sealed in a Teflon cup. The mixture was placed and tightly sealed in a steel container and transferred in a furnace at 175ºC for 48 h. A ligand exchange procedure with oleic acid was used to hydrophobise the synthesized nanoparticles. The nanoparticle suspension in benzyl alcohol was centrifuged once and the pellet resuspended in chloroform (5 mL). Oleic acid was then directly added in excess (50uL) into the nanoparticle solution which was then immediately placed in a sonic bath for 60 min. The oleic acid capped nanoparticles were washed three times using high speed centrifugation to remove excess oleic acid. The oleic acid capped nanoparticles were used as solid templates for the formation of core-shell micellar hybrid structures. Typically, 1mL of a mixture of 1,2-distearoyl-sn-glycero-3-phosphoethanolamine-N-[carboxyl (polyethylene glycol)] (DSPCE-PEG-COOH), 1,2-dimyristoyl-sn-glycero-3-

phosphoethanolamine-polyethylene glycol (DSPE-PEG) and L-alpha-phosphatidylcholine (PC) (20:50:30 %Weight 2mg/mL) in chloroform was prepared and mixed with the oleic acid capped nanoparticles (~10 umol Fe). To facilitate monitoring of cellular interactions, the lipophilic near-infrared (NIR) fluorescence probe *1,1*'-dioctadecyl-3,3,3',3'-tetramethyl indotricarbocyanine Iodide (DIR) was added to the phospholipid mixture (0.5% Weight). The solvent was evaporated at 55°C and the samples were stored under nitrogen at -20 °C until used. The dry nanoparticle film was heated to 70 °C and rehydrated with 1mL H_2O. Empty micelles were removed by a round of centrifugation at 14000 rpm and the pellet was resuspended in H2O. To enable conjugation with the J591 monoclonal antibodies, the terminal carboxyl groups of the DSPCE-PEG-COOH were activated using N-hydroxysuccinimide (NHS, 50mM) and N-(3-Dimethylaminopropyl)-N′-ethylcarbodiimide hydrochloride (EDC, 100mM) for 10min. The nanoparticle suspensions were centrifuged and resuspended into 1 mL of PBS and quickly added to the antibody solution (75 ug antibody per 10 umol Fe). The mixture was left to react overnight after which the antibody conjugated nanoparticles were purified by centrifugation at 4 °C. Hydrodynamic diameters and polydispersity indexes were determined using a Zetasizer Nano ZS equipped with a 633 nm He-Ne laser (Malvern Instruments). Transmission electron microscopy (TEM) measurements were conducted using a Philips CM100 TEM.

Cell lines

The human prostate cancer cell lines LNCaP, PC3, DU145, 22RV1 (all sourced from American Type Culture Collection (ATCC), USA), BPH-1 (from Dr Simon Hayward, Vanderbilt University Medical Center, USA), LNCaP-C42B (abbreviated C42B) (from Dr Leland Chung, Cedars-Sinai Medical Center, USA) [19, 20], LNCaP-LN3 (from Dr Curtis Pettaway, MD Anderson Cancer Center, University of Texas, USA) and LNCaP-luc (generated in-house) were maintained in RPMI media containing 5% fetal bovine serum. LNCaP-luc cells were generated using the

Viralpower Lentiviral gene expression system (Invitrogen, USA) according to the manufacturer's instructions. Briefly, supernatant containing the lentivirus was mixed with polybrene (8 μg/ml) and used to infect LNCaP cells. After infection, positive transfectants were selected as a pool by treatment with blasticidine (8 μg/ml) for six days. RWPE-1 cells (ATCC) were grown in keratinocyte serum-free media (SFM) supplemented with recombinant human epidermal growth factor (5 ng/mL final concentration) and bovine pituitary extract (50 ng/mL). The J591 hybridoma (from Dr Neil Bander, Weill Medical Centre, Cornell University, USA) which produces the anti-PSMA antibody [21], was maintained in Hybridoma SFM. All media and supplements were sourced from Gibco, Life Technologies. All cell lines were incubated at 37°C in a humidified atmosphere of 5% $C0_2$/air.

Purification of anti-PSMA antibody (J591) by affinity chromatography

The hybridoma J591 was cultured as described until the media were exhausted, and the secreted antibody was harvested. The hydridoma culture supernatant was passed through a HiTrap Protein HP column (GE Healthcare, UK) according to the manufacturer's instructions, on an AKTA FPLC system (GE Healthcare, UK). The bound IgG was eluted using 0.1 M glycine, pH 3, and the pH was immediately neutralized with 1 M Tris-base, pH 9.0. The eluates were dialysed against PBS and the purity of antibody preparations was determined by SDS-PAGE followed by Coomassie blue (Biorad, USA) staining. The concentration was determined by BCA protein assay (Pierce Biotechnology, USA).

Flow cytometric detection of PSMA

Cells were grown to 80% confluence in T75 flasks, washed twice in PBS then lifted using non-enzymatic cell dissociation buffer (Sigma Aldrich, USA). Cells were then washed in PBS containing 5% FBS (FACSWASH) then resuspended at 10^6 cells/mL. 100 μL of cell suspension were incubated with affinity-purified J591 antibody on ice for 1 hour, and then washed thrice

in FACSWASH. Cells were then incubated with a secondary AlexaFluor 488-labelled donkey anti-mouse IgG (H+L) antibody (Life Technologies, USA) for 30 mins on ice, before washing thrice in FACSWASH. Cells were then run on a FACS Canto (BD Bioscience, USA) and data analysed using Kaluza software (Beckman Coulter, USA).

Cell toxicity assays

The effect of MNPs on the viability of PCa cells was determined using Alamar blue reagent (Invitrogen, Life Technologies). Cells were seeded at 5,000 cells per well (100 µL volume) in a 96-well plate, and cultured overnight in growth media. Various amounts of MNPs in 100 µL volume were added to the wells (see Figure 2 legend for amounts), and plates were returned to the incubator for 48 hours. 20 µL of Alamar blue reagent were added to all wells, which were then incubated at 37^{o}C for 3-4 hours. 100 µL of supernatant were transferred to a black 96 well plate, and fluorescence at 590nm was measured using a FLUOstar Omega plate reader (BMG Labtech, Germany).

Prussian blue staining for uptake of MNPs

For *in vitro* studies, cells grown on chamberslides or on cover slips were incubated for 2 hours at room temperature with MNP alone, MNPs conjugated to J591 (J591-MNP) or J591 alone. Cells were fixed in 2% paraformaldehyde, washed with PBS, and then stained for iron using the Accustain reagent (Sigma Aldrich, USA) according to the manufacturer's instructions. Briefly, the cells were stained in Iron Staining solution for 10 minutes, rinsed in deionised water, and then counter-stained for 5 minutes in Pararosaniline solution for 5 minutes. The cells were rinsed in deionised water again, air-dried then mounted with a coverslip. For *in vivo* studies, all mice were euthanized immediately after MRI (approximately 24 hours post MNP injection), and the harvested tissues were fixed in 10% neutral buffered formalin for 48-72 hours and then in 70% ethanol for a further 48 hours. The tissues were then processed on

a Tissue-Tek VIP6 tissue processor, blocked in paraffin then sectioned at 5um thickness. The same Accustain protocol was used to perform iron staining of tissue sections.

Fluorescence microscopy

C42B cells grown on coverslips were incubated for 2 h at room temperature in the presence of MNPs alone, J591-MNP or J591 alone. Cells were washed, incubated with AlexaFluor-488 donkey anti-mouse antibody (Life Technologies, USA) for 30 minutes at room temperature, washed PBS and then fixed in 2% paraformaldehyde. Cells were then washed once with PBS, and coverslips were mounted onto slides. Images were acquired on a Zeiss confocal microscope.

Animal studies (orthotopic prostate xenograft model)

All studies were in accordance with guidelines of the Animal Ethics Committees of Queensland University of Technology (QUT) and The University of Queensland (UQ), and Australian Code for the Care and Use of Animals for Scientific Purposes. LNCaP or bioluminescent LNCaP-luc cells were lifted from culture flasks with trypsin, washed twice with PBS and resuspended in PBS. Cell counts were performed with a haemocytometer and viability was assessed by trypan blue exclusion. For intraprostatic injections, hair was removed from the abdomen of mice using a hair clipper, and the mice were anaesthetised with ketamine (25mg/kg) and xylazine (5mg/kg) and received buprenorphine (0.1mg/kg) for analgesia. An incision at the midline of the abdomen of NOD/SCID mice was made through the skin, exposing the dorsal prostate. $1x10^6$ LNCaP-luc cells were injected into the dorsal prostate in 25 µl volume. The bladder was returned to the abdomen and the incision closed with sutures. Tumor development was monitored by bioluminescence imaging using an IVIS Spectrum (Xenogen, USA) weekly for a total of 4 weeks after tumor cell implantation. For bioluminescence imaging, mice were injected intraperitoneally with D-luciferin diluted in PBS (15 mg/mL stock) at 150 mg/kg.

Mice were anaesthetised via isoflurane inhalationand imaged 8–12 minutes after injection with D-luciferin. Bioluminescence was analysed using Living Imagine software (Xenogen, USA).

Magnetic resonance imaging (MRI) studies (Pilot studies)

In experiments involving MRI on non-tumor bearing mice injected with MNPs directly into the prostate, mice were first anaesthetised with ketamine and xylazine. A small midline incision was made on the abdomen of NOD/SCID mice, exposing the dorsal prostate, and 12µg of MNPs in 20 µL volume were injected into it. MRI was performed 1h, 24h and 48 h thereafter. In experiments involving MRI on mice bearing orthotopic LNCaP or LNCaP-luc tumors, mice were injected with MNPs alone (n=2) or J591-MNP (n=3) intravenously via tail vein at 6 mg/kg and MRI was performed 2 h and 24 h thereafter. This dosage was based on similar studies that also involved tail vein injection of MNPs to enhance MRI of other cancer types in rodents [22-24]. The well-being of all mice throughout the duration of the experiments, particularly after MNP administration, was closely monitored. We employed the animal welfare assessment methodology by DB Morton [25]. All mice were euthanized by CO_2 asphyxiation immediately after their final MRI scan (24 h or 48 h, depending on experiment; see figure legends). Mice were imaged on a Bruker (Germany) AV700 MRI system consisting of a 16.4T vertical magnet interfaced to an AVANCE II spectrometer running Paravision 5 using a 25 mm volume coil in a micro2.5 gradient set, under isofluorane anaesthesia. Recirculating water in the gradient set was maintained at 30°C. A series of fast low-resolution gradient echo (GE) images were acquired as localisers for placement of the following image sets. A series of axial GE images, centred on the prostate, were acquired with typical parameters as follows: TR = 252 ms, TE = 2.8 ms, pulse angle 30°, field-of-view = 30X30 mm, matrix = 320X320, slice thickness 0.8 mm, slice gap = 0 mm, number of slices = 19, numbers of averages = 12, acquisition time = 16 min.

RESULTS

Characterisation of MNPs and J591 alone

The magnetic nanoparticle preparation was developed based on the solvent-evaporation method initially reported for the preparation of quantum dots phospholipid micellar hybrids [26]. Highly monocrystalline magnetite nanoparticles were synthesized using the one-pot benzyl alcohol route described by Niederberger *et al* and further phase-transferred into chloroform using oleic acid as a capping agent. The oleic acid coated nanoparticles were then mixed with PEGylated phospholipids and the solvent evaporated. Rehydration of the dry film yielded the phospholipid coated magnetic nanoparticles which could be easily purified from empty micelles using centrifugation. Terminal carboxylic groups on the 1,2-distearoyl-sn-glycero-3-phosphoethanolamine-N-[carboxyl (polyethylene glycol)] were activated using EDC/NHS and further reacted with the J591 antibody to yield the immune-targeted MNPs. Characterization of the nanoparticles was carried on using transmission electron microscopy and dynamic light scattering measurements which showed that the sample consisted of small clusters of the magnetic nanoparticles (Figure 1A). The mean hydrodynamic diameter of the MNP clusters was 110 nm and the polydispersity index 0.127 as determined using dynamic light scattering (Figure 1B). Affinity-purified J591 antibody was shown to be specific for PSMA through binding only to known PSMA-positive cell lines (22RV1, LNCaP, and C42B cells) but not to those that are PSMA-negative (BPH-1, RWPE-1 and DU145 cells) as determined by flow cytometry (Figure 1C).

MNPs are non-toxic to prostate cancer cells,

To determine if MNPs has any toxic effects on cells, RWPE-1 cells (non-tumorigenic prostate cell line), LNCaP, C42B, PC3 and DU145 cells (tumorigenic cell lines) were incubated with various doses of MNPs alone for 48 hours. The viability of cells was not affected, as assessed by Alamar blue reagent (Figure 2).

J591-MNP led to increased tumor uptake of iron, and binding of J591 to PSMA is not compromised when conjugated to MNPs

To assess whether or not conjugation of MNPs with J591 facilitates iron uptake by tumors *in vitro*, C42B cells (PSMA-positive) were incubated with MNP alone or J591-MNP. Confocal microscopy shows minimal iron uptake in cells treated with MNPs alone, but significant uptake was seen with J591-MNP (Figure 3A). The J591 component of J591-MNP could also be visualised with the FITC-labelled anti-mouse secondary antibody. Similarly, Prussian blue staining showed greater iron uptake by LNCaP-LN3 cells (PSMA-positive) *in vitro* when incubated with J591-MNP than with MNP alone (Figure 3B top panel), confirming that conjugation of MNPs to J591 facilitated their uptake by the prostate cancer cells. The immunohistochemical staining intensity for PSMA by J591-MNP was similar to that of J591 alone, indicating that conjugation of MNP did not compromise antibody binding to PSMA (Figure 3B bottom panel).

Direct injection of MNPs into the prostate of mice induces negative contrast on MR images

To provide proof-of-concept that the presence of MNPs within the prostate is detectable by MRI, non tumor-bearing mice were injected with MNPs alone directly into their normal prostate. MR images taken 1 hour after MNP injection showed significant darkening at that anatomical site. A similar degree of negative contrast was seen in the same mouse on MRI images taken 24 hours and 48 hours post-MNP injection (Figure 4). The darkening effect as a result of the MNP facilitated the visualisation and localisation of the prostate.

Enhanced MRI of orthotopic xenograft LNCaP tumors by J591-MNP (Pilot study)

To evaluate the potential of PSMA-targeting MNPs as an imaging agent for MRI of prostate cancer, MRI was performed on mice with pre-established orthotopic LNCaP-luc tumors and

intravenously injected with either MNPs alone or J591-MNPs. MR images of tumors from mice that received the J591-MNP conjugates showed significant darkening at the prostate region, at the 2-hour and 24-hour post-injection timepoints (Figure 5). Negligible darkening effect was observed in mice that received intravenous MNPs alone (Figure 5). Prussian blue staining of resected tumors from J591-MNP mice showed significant accumulation of iron within the tumor. In contrast, little iron accumulation was seen in the tumors from the MNP alone group (Figure 6), suggesting improved tumor targeting by the conjugates. Iron uptake was strong in the spleens of all mice, independent of treatment group (Figure 6). A low level of iron uptake was seen in the liver of all mice, with no difference between the two groups.

DISCUSSION

PCa is currently imaged using MRI, TRUS and nuclear medicine [27]. However, these imaging techniques do not provide adequate detection for small tumor volumes or lymph node involvement [2]. The ability to accurately detect and locate small tumors is necessary for early detection of disease and for assessment of response to therapy in cancer patients. In recent years, the use of biomarker-targeted probes linked with nanoparticle-based contrast agents to enhance these imaging modalities has been a major area of research. In this study, we provide proof-of-concept that iron oxide MNPs conjugated with the PSMA-targeting antibody, J591, enhances MRI of prostate cancer in a preclinical model of orthotopic prostate cancer xenografts in mice.

MRI is a highly desirable imaging technology because it is non-invasive, provides excellent soft tissue contrast, multidimensional morphological information, and does not involve exposure to ionising radiation [1]. MRI can be strongly enhanced through the employment of MNPs [1]. The presence of magnetic cores within the tissues decreases the relaxation times of the protons of surrounding water, causing a darkening effect at those sites in MR imaging. We showed that direct injection of MNPs into the prostate of mice (Figure 4) or intravenous injection of PSMA-targeting MNPs which homed to the orthotopic tumors (Figure 5), caused darkening at those anatomical locations in MR images. These observations have major clinical implications because tumor-targeting MNPs could potentially enable the early detection of tumors confined within the prostate by MRI. Although PSMA is expressed also on normal prostate cells, the level is significantly lower as compared to malignant cells. In addition, and very importantly, small metastases in lymph nodes and bone metastases may also be visualised using this technique. A key point is that lesions identified through our MNP-

assisted MRI approach are prostate-derived. Currently, MRI and CT use lymph node size to distinguish between those that are malignant or benign, an approach based on the premise that the enlargement of nodes is due to the accumulation of metastatic cells [28]. However, not all enlarged lymph nodes contain tumor cells, and normal-sized lymph nodes can also harbour metastases, hence false-positives and false-negatives remain as limitations. MNP-enhanced MRI could potentially facilitate accurate nodal staging, independent of node size, an important prognostic factor [28]. Bone metastases are currently identified through radionuclide bone scans, and in the future this approach could be complemented with MNP-enhanced MRI.

An important consideration in the design of biomarker-targeting imaging probes is the biological characteristics of the biomarker itself. PSMA is an excellent prostate tumor biomarker to target for a number of reasons. Its expression is highly restricted to prostatic cells, although it has also been reported to be expressed on endothelial cells, and its level increases with higher cancer stages [29]. Unlike prostate specific antigen (PSA), the clinically used biomarker of prostate cancer, PSMA is still expressed on tumors from patients undergoing androgen deprivation therapy. But very importantly, the cytoplasmic domain of PSMA contains a novel motif of amino acid sequence MXXXL, that mediatesits internalisation and endosomal recycling via a clathrin-dependent mechanism [13, 14]. This leads to high intracellular uptake of ligands carrying nanoparticles such as MNPs or other compounds, an important quality that improves tumor imaging due to the retention of the contrast agent for longer duration. Indeed, we found that the MNP-mediated darkening effect on MR images lasted for at least 24 hours in live mice (Figure 5). The specificity of the targeting agent is also very important in the design of biomarker-targeting imaging probes. In this study, we used the J591 monoclonal antibody due to its well established specificity. ^{177}Lu-J591 was been

previously shown in a Phase II clinical trial to target all known sites of disease in all treated subjects [15]. In another study, treatment of patients with ^{111}In-J591 and then with ^{90}Y-J591 revealed 89% of known bony metastases and 69% of soft tissue lesions [16]. The high specificity of J591 for PSMA was also confirmed by us using flow cytometric analysis of a panel of prostate cancer cell lines with known PSMA expression status (Figure 1B). When J591 was conjugated with our MNPs, the binding ability of the antibody to PSMA was not compromised (Figure 3), which collectively suggests that our imaging platform is stable, and shows promise for translation into the clinic. MNPs also have the potential to be easily adapted to other imaging technologies such as nuclear or optical modalities, to provide anatomical, functional and molecular information [3].

Another major issue in the translation of nanotechnology into biomedical practice is the biocompatibility of the nanoparticles. MNPs have been demonstrated to be biocompatible and biodegradable [1]. It is suggested that following internalisation into cells, iron oxide cores degrade into iron ions which then incorporate into the haemoglobin pool [30]. In addition, coating of MNPs with biodegradable polymers such as dextran or PEG prevents agglomeration, which also improves biocompatibility [3]. In our own hands, MNPs did not affect the viability of a panel of prostate cell lines, including both benign and cancerous cell lines (Figure 2), and the well-being of mice 24-hours after MNP injection was not compromised (no changes to body weight, reflex, alertness, breathing rates, coating appearance, faecal texture etc… as compared to pre-injection; see Materials and Methods for details)".. Currently, ferumoxil (GastroMARK), an iron oxide-based MNPs formulation, is approved for use in clinical MRI to enhance imaging of the bowel. However, there have been some reports of unwanted side-effects in MNP usage. Feridex, a formerly FDA-approved MNP agent administrated intravenously for imaging of the reticuloendothelial system that is based

on the engulfment of MNPs by phagocytes, is known to cause back and groin pain, as well as inducing allergic reactions [31]. It is inevitable that intravenously injected MNPs, even those labelled with ligands to bind cell surface markers on cancer cells, will distribute to other body parts such as spleen and liver. From a clinical point of view, it is crucial to modify the MNPs (eg PEGylation) to limit their toxicity, and direct them to the anatomical site of interest via the attachment of a ligand to a cell surface tumor biomarker to improve imaging at that site. If efficient targeting is achieved, a lower overall dose could be used to create a good MRI signal, and therefore with lower potential side-effects.We found that when mice were injected with the targeted-MNPs, there was high iron uptake by the tumor, in contrast to those given non-targeted MNPs, which had negligible uptake (Figure 6). This correlated with the enhanced imaging (negative contrast) of orthotopic tumors by J591-MNP (Figure 5). None of the tumors from either group were hemorrhagic, further confirming that the stronger signals seen in J591-MNP tumors were indeed due to greater MNP uptake from PSMA-targeting, and not from them being hemorrhagic (higher iron content). We also found that iron uptake was high in the spleens of mice, with no difference in the level between the two treatment groups (Figure 6). This finding is not surprising as only a small percentage of PSMA-targeting MNPs is expected to accumulate within the tumor, with the remaining distributing through the whole body. There was also no difference in liver iron uptake between targeting and non-targeting MNPs groups (Figure 6), likely for the same reason. The level of uptake in the liver was lower than in the spleen, which is an intriguing finding since preferential liver uptake is usually observed for nanoparticles after intravenous administration. It might be related to the physicochemical properties of the phospholipid coated nanoparticles used in this study [32] and warrants further investigation.

The use of nanoparticles as contrast agents for MRI of prostate cancer has been investigated by other groups as well. Abdolahi *et al* used a similar approach to us in that J591 was conjugated to MNPs, and showed that this complex enhanced MRI of LNCaP (PSMA-proficient) but not DU145 (PSMA-deficient) cells [33]. These results are consistent with ours, although their study was limited to *in vitro* work only. Tan *et al.* reported that conjugation of CLTI peptide, which is specific to fibrin-fibronectin complexes in stroma, provided MRI contrast enhancement of subcutaneous PC3 xenografts in mice [34]. While this approach did not target prostate cancer cells *per se*, it still effectively enhanced MR detection of these tumors with good contrast-to-noise ratio. Gao *et al*. designed a theranostics technology for prostate cancer, whereby MNPs conjugated with docetaxel and a single-chain antibody against prostate stem cell antigen [35]. When injected in mice bearing PC3M xenografts, the nanoparticles provided MRI negative contrast, as well as inhibited tumor growth and prolonged their survival. Together with the promising data presented here, this body of work confirm the relevance of immunotargeting-superparamagnetic nanoparticles towards improving MR imaging of prostate cancer.

CONCLUSION

We provide proof-of-concept that PSMA-targeted MNPs can effectively enhance MRI of prostate cancer in a preclinical model of the disease. Based on its biocompatibility, stability, together with its ability to enhance MRI, PSMA-targeting MNPs have promise to be translated into the clinic to improve the management of prostate cancer.

FUTURE PERSPECTIVE

MRI will continue to be a major imaging tool for prostate cancer over the next decade due to its many desirable features as discussed above. However, as there has been an explosion in interest in the application of nanotechnology to improve imaging methods in recent years, we anticipate that some of the exciting and innovative strategies currently in development will be translated into the clinic in the short to medium-term future, and indeed improve the management of cancer. In particular, strategies involving the use of biomarker-targeted probes linked with nanoparticle-based contrast agents to enhance cancer imaging have great potential for diagnosis, staging (lymph node involvement) and for real-time imaging of treatment response.

ACKNOWLEGEMENTS

This project has been supported by Cancer Australia and Prostate Cancer Foundation of Australia (NHMRC-510239 and PG-0409). The authors wish to thank Mrs Susan Johnson for technical assistance with some experiments.

Executive Summary
Current status of prostate cancer imaging in the clinic
• MRI is routinely used for imaging of prostate cancer (PCa); however, improvements in tumor specificity and sensitivity are required especially for small tumors.
Development of a novel contrast agent to enhance MRI of PCa
• PSMA is a cell surface membrane protein expressed highly on PCa but minimally on normal prostate tissue (ideal imaging target). • The superparamagnetic effect of iron oxide magnetic nanoparticles (MNPs) provides negative contrast in MRI. • In this study, we conjugated the PSMA-specific antibody, J591, to MNPs. The

antibody delivers the MNP specifically to prostate cancer cells, while the MNP component provides negative contrast in MRI.

Key findings of our nanoparticle-antibody system for MRI

- MNPs did not affect the viability of prostate cancer cells *per se*, and were well tolerated by mice after injection.
- Significantly greater tumor uptake of MNPs occurred when they were labelled with J591, both *in vitro* and *in vivo,* than non-targeted MNPs.
- Importantly, J591-labelled MNPs localised to pre-established orthotopic tumors in mice, enhancing their detection by MR. High accumulation of iron was seen in these tumors; negligible accumulation for control group.

The big picture

- Our system has the potential to enhance PCa detection and localization in real-time, improving patient management.

REFERENCES

1. Yigit MV, Moore A, Medarova Z: Magnetic nanoparticles for cancer diagnosis and therapy. *Pharmaceutical research* 29(5), 1180-1188 (2012).
2. Taneja SS: Imaging in the diagnosis and management of prostate cancer. *Reviews in urology* 6(3), 101-113 (2004).
3. Liu G, Gao J, Ai H, Chen X: Applications and potential toxicity of magnetic iron oxide nanoparticles. *Small* 9(9-10), 1533-1545 (2013).
4. Pouliquen D, Le Jeune JJ, Perdrisot R, Ermias A, Jallet P: Iron oxide nanoparticles for use as an MRI contrast agent: pharmacokinetics and metabolism. *Magn Reson Imaging* 9(3), 275-283 (1991).
5. To SY, Castro DJ, Lufkin RB, Soudant J, Saxton RE: Monoclonal antibody-coated magnetite particles as contrast agents for MR imaging and laser therapy of human tumors. *J Clin Laser Med Surg* 10(3), 159-169 (1992).
6. Mahmoudi M, Serpooshan V, Laurent S: Engineered nanoparticles for biomolecular imaging. *Nanoscale* 3(8), 3007-3026 (2011).
7. Israeli RS, Powell CT, Fair WR, Heston WD: Molecular cloning of a complementary DNA encoding a prostate-specific membrane antigen. *Cancer Res* 53(2), 227-230 (1993).
8. Grauer LS, Lawler KD, Marignac JL, Kumar A, Goel AS, Wolfert RL: Identification, purification, and subcellular localization of prostate-specific membrane antigen PSM' protein in the LNCaP prostatic carcinoma cell line. *Cancer Res* 58(21), 4787-4789 (1998).
9. Schmittgen TD, Teske S, Vessella RL, True LD, Zakrajsek BA: Expression of prostate specific membrane antigen and three alternatively spliced variants of PSMA in prostate cancer patients. *Int J Cancer* 107(2), 323-329 (2003).
10. Wright GL, Jr., Grob BM, Haley C *et al.*: Upregulation of prostate-specific membrane antigen after androgen-deprivation therapy. *Urology* 48(2), 326-334 (1996).
11. Ghosh A, Heston WD: Tumor target prostate specific membrane antigen (PSMA) and its regulation in prostate cancer. *Journal of cellular biochemistry* 91(3), 528-539 (2004).
12. Wright GL, Jr., Haley C, Beckett ML, Schellhammer PF: Expression of prostate-specific membrane antigen in normal, benign, and malignant prostate tissues. *Urol Oncol* 1(1), 18-28 (1995).
13. Liu H, Rajasekaran AK, Moy P *et al.*: Constitutive and antibody-induced internalization of prostate-specific membrane antigen. *Cancer Res* 58(18), 4055-4060 (1998).
14. Rajasekaran SA, Anilkumar G, Oshima E *et al.*: A novel cytoplasmic tail MXXXL motif mediates the internalization of prostate-specific membrane antigen. *Molecular biology of the cell* 14(12), 4835-4845 (2003).
15. Bander NH, Milowsky MI, Nanus DM, Kostakoglu L, Vallabhajosula S, Goldsmith SJ: Phase I trial of 177lutetium-labeled J591, a monoclonal antibody to prostate-specific membrane antigen, in patients with androgen-independent prostate cancer. *J Clin Oncol* 23(21), 4591-4601 (2005).
16. Milowsky MI, Nanus DM, Kostakoglu L, Vallabhajosula S, Goldsmith SJ, Bander NH: Phase I trial of yttrium-90-labeled anti-prostate-specific membrane antigen monoclonal antibody J591 for androgen-independent prostate cancer. *J Clin Oncol* 22(13), 2522-2531 (2004).
17. Nicola Pinna SG, Pablo Beato ,Pierre Bonville , Markus Antonietti,and Markus Niederberger Magnetite Nanocrystals: Nonaqueous Synthesis, Characterization, and Solubility. *Chemistry of Materials* 17(11), 3044-3049 (2005).
18. Thierry B. A-EF, Brown M., Majewski P., Griesser H.J.: Immunotargeting of advanced functional nanostructures for cancer diagnosis and treatment. *Advanced Materials* 21, 541-545 (2009).
19. Thalmann GN, Anezinis PE, Chang SM *et al.*: Androgen-independent cancer progression and bone metastasis in the LNCaP model of human prostate cancer. *Cancer Res* 54(10), 2577-2581 (1994).
20. Wu TT, Sikes RA, Cui Q *et al.*: Establishing human prostate cancer cell xenografts in bone: induction of osteoblastic reaction by prostate-specific antigen-producing tumors in athymic and SCID/bg mice using LNCaP and lineage-derived metastatic sublines. *Int J Cancer* 77(6), 887-894 (1998).
21. Liu H, Moy P, Kim S *et al.*: Monoclonal antibodies to the extracellular domain of prostate-specific membrane antigen also react with tumor vascular endothelium. *Cancer Res* 57(17), 3629-3634 (1997).

22. Chen H, Wang L, Yu Q *et al.*: Anti-HER2 antibody and ScFvEGFR-conjugated antifouling magnetic iron oxide nanoparticles for targeting and magnetic resonance imaging of breast cancer. *Int J Nanomedicine* 8, 3781-3794 (2013).
23. Schleich N, Sibret P, Danhier P *et al.*: Dual anticancer drug/superparamagnetic iron oxide-loaded PLGA-based nanoparticles for cancer therapy and magnetic resonance imaging. *Int J Pharm* 447(1-2), 94-101 (2013).
24. Bu L, Xie J, Chen K *et al.*: Assessment and comparison of magnetic nanoparticles as MRI contrast agents in a rodent model of human hepatocellular carcinoma. *Contrast Media Mol Imaging* 7(4), 363-372 (2012).
25. Morton: Human endpoints in animal experiments for biomedical research: ethical, legal and practical aspects. Royal Society of Medicine Press (1999).
26. Dubertret B, Skourides P, Norris DJ, Noireaux V, Brivanlou AH, Libchaber A: In vivo imaging of quantum dots encapsulated in phospholipid micelles. *Science* 298(5599), 1759-1762 (2002).
27. Kelloff GJ, Choyke P, Coffey DS: Challenges in clinical prostate cancer: role of imaging. *AJR. American journal of roentgenology* 192(6), 1455-1470 (2009).
28. Harisinghani M: Nanoparticle-enhanced MRI: are we there yet? *Lancet Oncol* 9(9), 814-815 (2008).
29. Osborne JR, Akhtar NH, Vallabhajosula S, Anand A, Deh K, Tagawa ST: Prostate-specific membrane antigen-based imaging. *Urol Oncol* 31(2), 144-154 (2013).
30. Thorek DL, Chen AK, Czupryna J, Tsourkas A: Superparamagnetic iron oxide nanoparticle probes for molecular imaging. *Annals of biomedical engineering* 34(1), 23-38 (2006).
31. Colombo M, Carregal-Romero S, Casula MF *et al.*: Biological applications of magnetic nanoparticles. *Chemical Society reviews* 41(11), 4306-4334 (2012).
32. Bertrand N, Leroux JC: The journey of a drug-carrier in the body: an anatomo-physiological perspective. *J Control Release* 161(2), 152-163 (2012).
33. Abdolahi M, Shahbazi-Gahrouei D, Laurent S *et al.*: Synthesis and in vitro evaluation of MR molecular imaging probes using J591 mAb-conjugated SPIONs for specific detection of prostate cancer. *Contrast Media Mol Imaging* 8(2), 175-184 (2013).
34. Tan M, Burden-Gulley SM, Li W *et al.*: MR molecular imaging of prostate cancer with a peptide-targeted contrast agent in a mouse orthotopic prostate cancer model. *Pharmaceutical research* 29(4), 953-960 (2012).
35. Gao X, Luo Y, Wang Y *et al.*: Prostate stem cell antigen-targeted nanoparticles with dual functional properties: in vivo imaging and cancer chemotherapy. *Int J Nanomedicine* 7, 4037-4051 (2012).

FIGURES

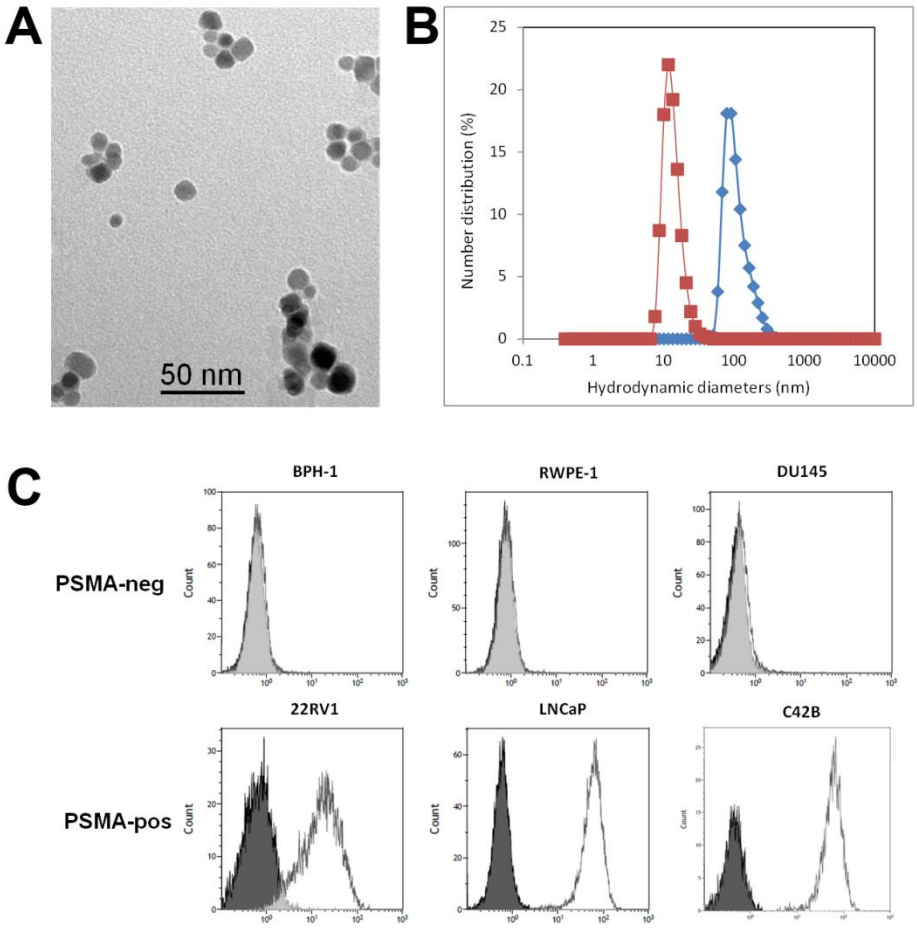

Figure 1. Characterisation of MNPs and J591 separately. **A**) TEM image of the MNPs as small aggregates. B) Hydrodynamic diameters of the iron oxide MNPs as synthesised (red line) and with the PEG-DSPE coating (blue line; abbreviated as MNPs). **C**) Flow cytometric analysis showed that the J591 antibody binds specifically to PSMA because positive staining was only detectable on PSMA-positive prostate cancer cells (22RV1, LNCaP and C42B) but not on PSMA-negative cells (BPH-1, RWPE-1, and DU145).

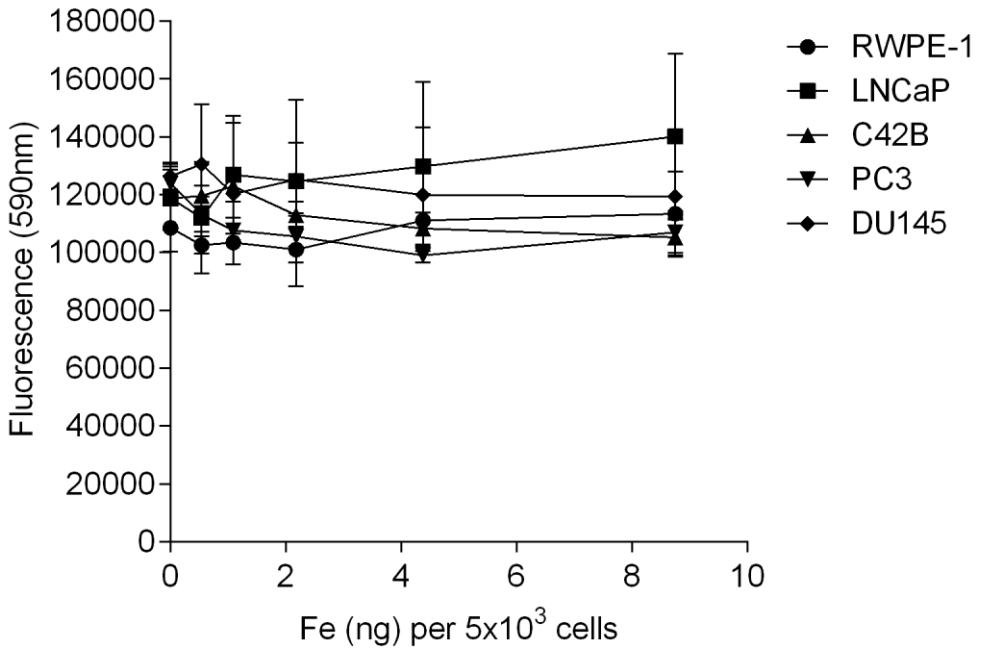

Figure 2. MNPs are non-toxic to prostate cancer cells. Incubation of prostate cancer cell lines with various amounts of MNPs alone for 48 hours did not affect their viability, as assessed by Alamar blue viability assay.

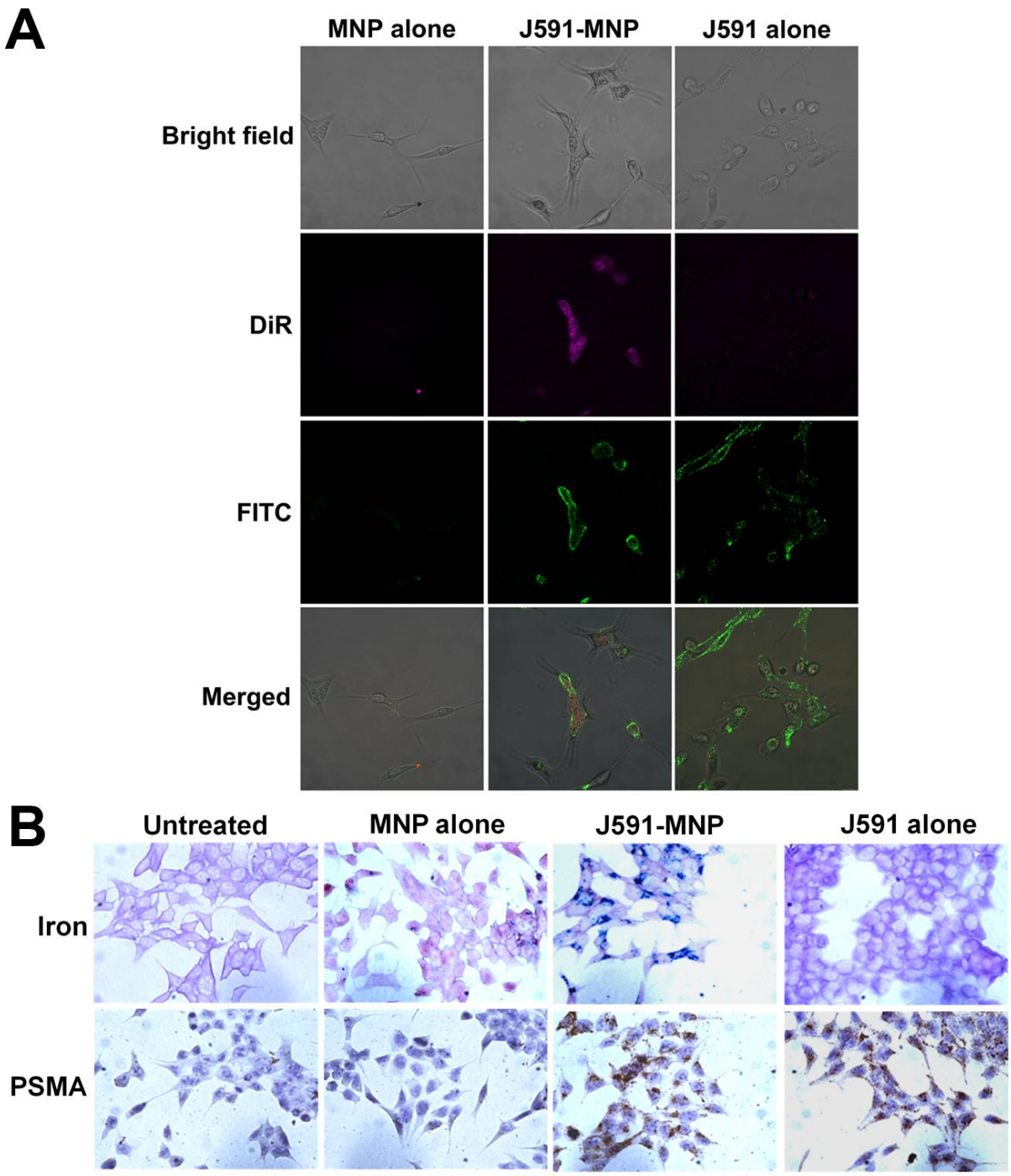

Figure 3. J591-MNP led to increased tumor uptake of iron, and binding of J591 to PSMA is not compromised when conjugated to MNPs. **A**) Confocal images of C42B cells after incubation with MNPs alone, J591-MNP or J591 alone, show that uptake of MNPs (DiR-labelled; purple) is increased when conjugated to J591. The J591 component of J591-MNP could be visualised with the FITC-labelled secondary antibody. Images were acquired on a Zeiss confocal microscope. **B)** Prussian blue staining for iron (top panel; dark blue) showing

greater iron uptake by LNCaP-LN3 cells with J591-MNP than MNP alone. Immunohistochemical staining for PSMA (bottom panel) shows that both J591-MNP, and J591 alone, give the same level of staining on LNCaP-LN3 cells, indicating that conjugation of MNPs to J591 does not affect its binding and specificity for PSMA. Minimal staining was seen with MNP alone.

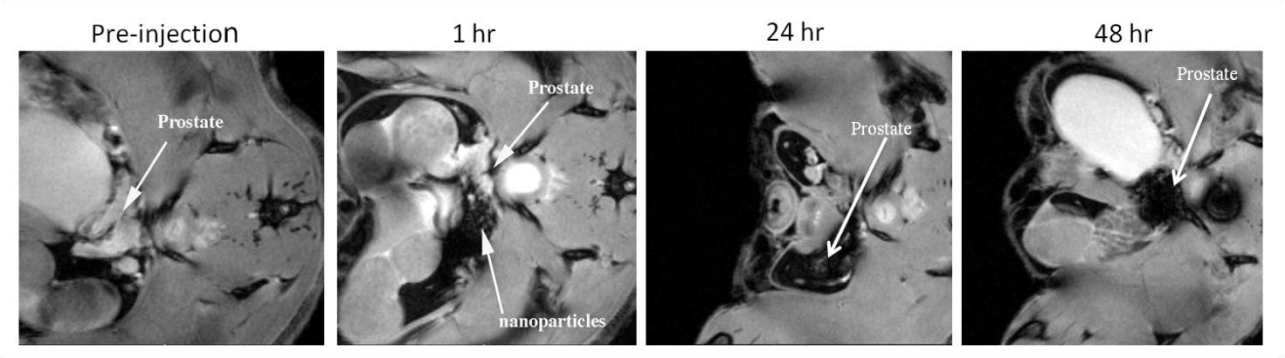

Figure 4. **Direct injection of MNPs into the prostate of non-tumor bearing mice causes darkening of MR images of the prostate**. The prostate appears white/pale in MR images taken prior to MNP injection, but it appears black and granulated on MR images once MNP was injected (12ug of MNP in 20ul volume). This negative contrast effect was seen after 1-, 24- and 48-hours post-MNP injection in the same live mouse. MR images of a representative mouse are shown.

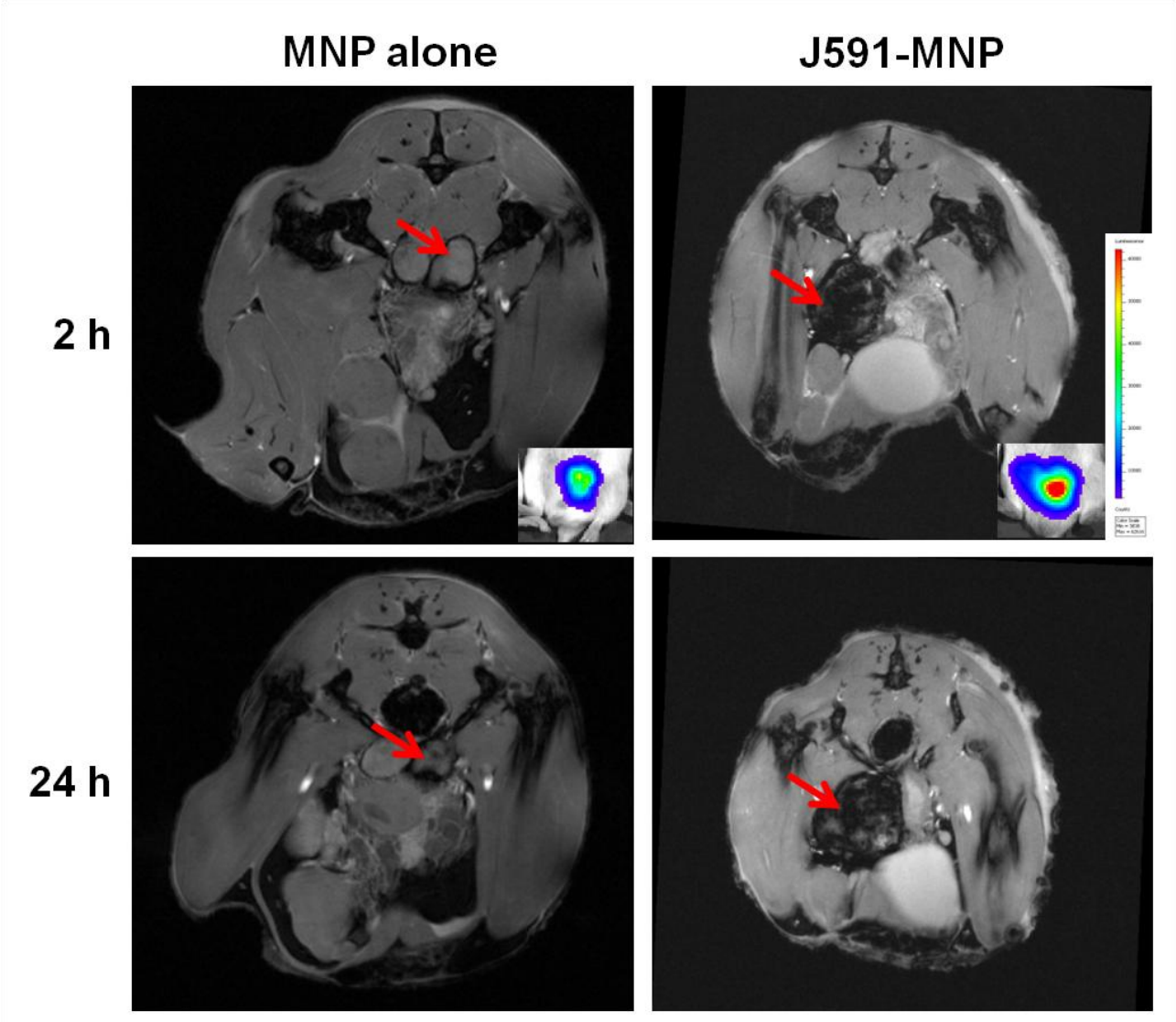

<u>Figure 5:</u> Enhancement of MRI with targeted MNP-J591 (pilot study). Once the pre-established LNCaP-luc tumors had reached the desired size (based on bioluminescence signal; inset), which occurred approximately 4-weeks post tumor cell injection, the mice were injected intravenously with MNPs alone (n=2) or J591-MNP (n=3). Administration of J591-MNP conjugates resulted in significant darkening of MR images of the prostate region, at 2- and 24-h post-injection. No darkening effect occurred in mice given MNPs alone. Red arrows: orthotopic LNCaP-luc tumors. MR images of representative mice from each group are shown.

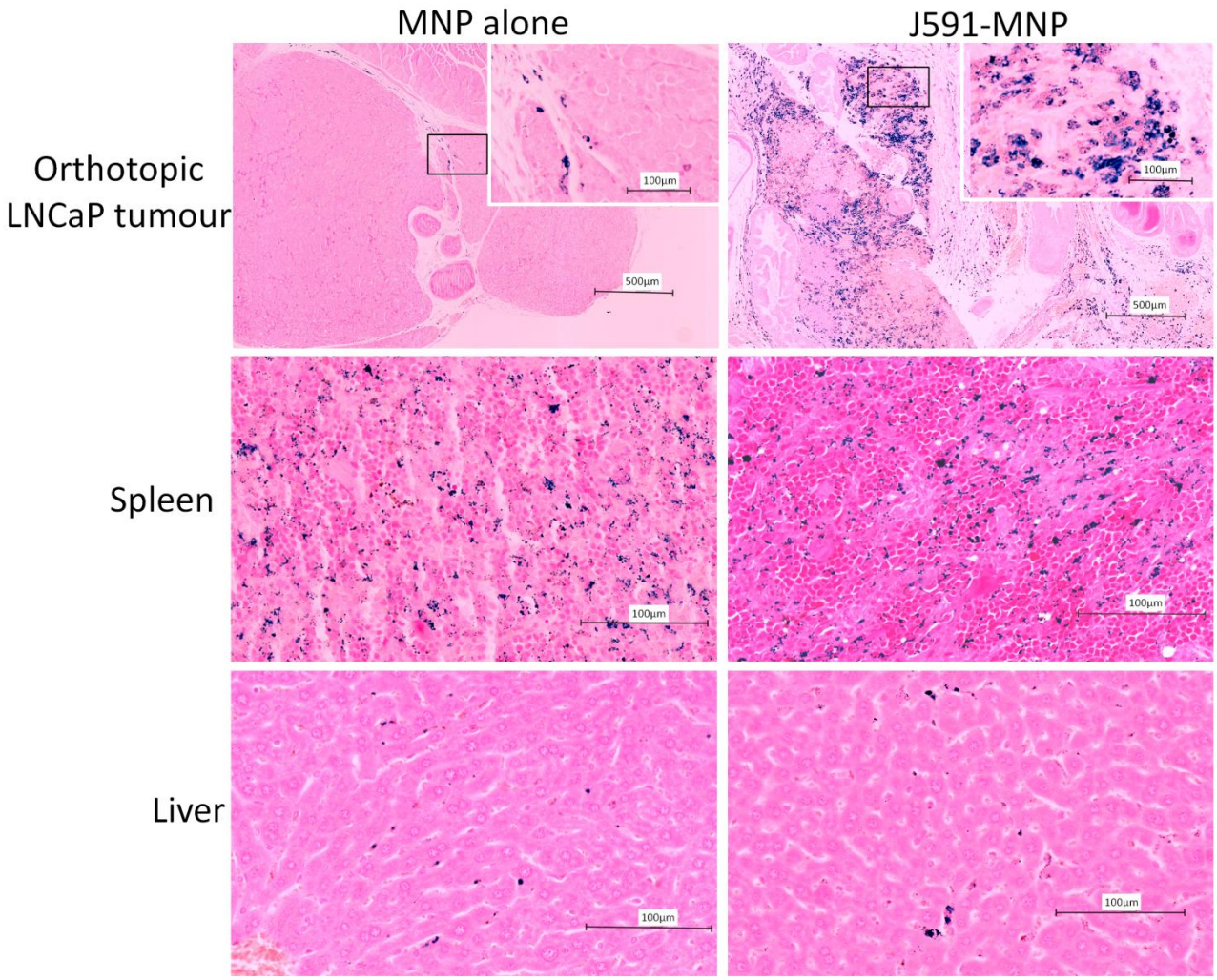

<u>Figure 6:</u> Targeting of orthotopic tumors is improved when J591 is conjugated to MNPs. Prussian blue staining showed significant iron uptake in resected LNCaP tumors from mice injected intravenously with J591-MNP (n=5), as compared to MNP alone (n=4). Similar high levels of iron uptake is observed in the spleens between J591-MNP and MNP alone mice. Low iron uptake was seen in liver from all mice.